

Spin-Polarized Electron Transport at Ferromagnet/Semiconductor Schottky Contacts

J. D. Albrecht

Air Force Research Laboratory, Wright-Patterson AFB, Ohio 45433

D. L. Smith

Los Alamos National Laboratory, Los Alamos, New Mexico 87545

We theoretically investigate electron spin injection and spin-polarization sensitive current detection at Schottky contacts between a ferromagnetic metal and an n-type or p-type semiconductor. We use spin-dependent continuity equations and transport equations at the drift-diffusion level of approximation. Spin-polarized electron current and density in the semiconductor are described for four scenarios corresponding to the injection or the collection of spin polarized electrons at Schottky contacts to n-type or p-type semiconductors. The transport properties of the interface are described by a spin-dependent interface resistance, resulting from an interfacial tunneling region. The spin-dependent interface resistance is crucial for achieving spin injection or spin polarization sensitivity in these configurations. We find that the depletion region resulting from Schottky barrier formation at a metal/semiconductor interface is detrimental to both spin injection and spin detection. However, the depletion region can be tailored using a doping density profile to minimize these deleterious effects. For example, a heavily doped region near the interface, such as a delta-doped layer, can be used to form a sharp potential profile through which electrons tunnel to reduce the effective Schottky energy barrier that determines the magnitude of the depletion region. The model results indicate that efficient spin-injection and spin-polarization detection can be achieved in properly designed structures and can serve as a guide for the structure design.

PACS numbers: 85.75.-d, 73.50.-h, 73.40.Qv, 73.30.+y

I. INTRODUCTION

Semiconductor physics is in the midst of a wide ranging exploration of physical phenomena and device concepts that are connected with the electron spin degree of freedom. Much work has focused on optical generation and detection of spin populations. However, most spin based device concepts require an electrical means of injecting, manipulating, and detecting spin-polarized electron currents. Thus it is important to understand the fundamental physics of electron spin transport in the main structural components that make up semiconductor devices. The Schottky contact is an essential semiconductor device component. Schottky contacts form at most metal/semiconductor interfaces. Electrical spin injection and detection schemes often involve ferromagnetic metal/semiconductor interfaces with Schottky contacts so it is important to understand spin dependent electron transport at these structures.

Presently, theories for the injection or detection of spin-polarized electron currents at a metallic ferromagnet/nonmagnetic semiconductor interface have been formulated in the spirit of transport at a ferromagnetic metal/normal metal interface. The description of spin transport is incorporated using variations on a spin diffusion equation.¹ In these approaches^{2,3,4,5,6,7} the semiconductor is described as a poorly conducting metal, in the sense that the carrier density and thus the conductivity of the semiconductor is taken to be spatially uniform. Important insights gained through these models include: (i) the large conductivity mismatch between a highly conductive metal and a comparatively weakly conductive semiconductor is a major obstacle to spin injection; and (ii) a spin selective interface resistance can be of great benefit to efficient spin injection. A major drawback to a spin device physics model based on such uniform conductivity treat-

ments is that they do not describe the underlying electronic properties, the currents and potentials of real semiconductor structures. An obvious example of a problem with uniform conductivity models for metal/semiconductor Schottky contacts is that they yield the symmetric, linear current-voltage characteristics of resistors rather than the rectifying characteristics of diodes. An initial study of spin injection including the effects of band-bending in a depletion region at an n-type Schottky contact showed that the depletion region can have an important effect on spin transport and that a device-physics approach to the theory of spin-contacts is necessary.⁸

Experimentally, spin dependent transport has been investigated at interfaces consisting of a ferromagnetic metal^{9,10,11} or a heavily doped spin-polarized semiconductor^{12,13} contact and a non-magnetic semiconductor. Both spin injection, in which the electron flux flows from the spin polarized contact into the nonmagnetic semiconductor, and spin detection, in which the electron flux flows from the nonmagnetic semiconductor into the spin polarized contact, have been considered. In the spin injection measurements, detection of spin-polarized injection is often made using a spin-LED (light-emitting diode) configuration. In these experiments, electrons are injected into an n-type semiconductor from a spin polarized contact and are subsequently transported to a detection region, typically a quantum well, where they recombine with unpolarized holes transported from an adjacent p-type doped region. Because of the optical selection rules in III-V semiconductors the relative intensity of right- and left- circularly polarized luminescence gives a measure of the spin-polarization of the electron density in the recombination region. In spin detection measurements, spin polarized electrons are often optically generated in III-V semiconductors, and a spin dependent voltage signal is sought as the electron flux is transported into a spin polarized contact.

In this paper, we theoretically investigate spin-polarized

electron current at ferromagnetic metal/semiconductor Schottky contacts. We systematically treat the semiconductor device operation and the spin physics at the same level of approximation. We consider both n-type and p-type Schottky contacts with current flow corresponding to either forward and reverse bias. We first treat the overall electrostatics of the system and subsequently solve charge and spin continuity equations. We use a drift-diffusion transport model to describe the charge and spin currents. The drift-diffusion transport model is a strong scattering approximation appropriate for relatively high temperatures, such as room temperature. It is the approach used to describe most semiconductor device operation. Here we extend this approach to describe spin dependent transport at Schottky contacts. We find that the depletion region associated with a Schottky energy barrier can have a very strong effect on spin-polarized electron transport at ferromagnetic metal/semiconductor contacts. A large Schottky barrier is detrimental to spin injection and can also hinder spin detection. The model suggest structure design strategies for reducing the detrimental effects of the Schottky energy barrier.

The paper is organized in the following way: in Sec. II we describe the model, in Sec. III we present our numerical results and in Sec. IV we summarize our conclusions. Calculational details are included in the appendices.

II. DESCRIPTION OF MODEL

When a metal/semiconductor interface is formed the Fermi energy is usually pinned within the energy gap of the semiconductor. The position of the the semiconductor valence and conduction bands, relative to Fermi energy, at the interface does not depend strongly on the bulk doping of the semiconductor or on which metal is used to make the contact. For a given semiconductor, this energy matching position at the interface is largely fixed. Generally the position of the semiconductor valence and conduction bands relative to the Fermi energy at the interface, which depends on interfacial charge distribution, does not coincide with the corresponding energy position of the bands in the bulk of the semiconductor, which depends on the bulk doping level. There is a band bending region near the interface which at zero applied bias: is depleted of carriers, is charged because of the background doping, and has a large spatially varying electric field. The Schottky energy barrier between the pinned Fermi level and the semiconductor conduction band at the interface results in the charged depletion region and has important consequences on charge current flow at metal/semiconductor interfaces. For example, it leads to diode type current-voltage characteristics. Thus, it is not particularly surprising that this energy barrier and depletion region also have important consequences on spin current flow at these interfaces.

The design of the interface is central to spin injection and detection structures. In particular, spin dependent interface resistance resulting from spin dependent tunnel barriers have been argued to be essential for effective spin injection or detection at metal semiconductor interfaces.^{4,5,6} Possible spin-selective interface resistance layers, formed from thin mag-

netic insulators, have been experimentally investigated by Motsnyi, et al.¹⁴ In other work, Hanbicki, et al., have investigated Schottky barriers with heavy doping near the interface to study structures in which current is dominated by tunneling for spin injection.¹⁵ These results are promising for the realization of future electron spin based device designs. Interfacial spin-flip scattering, which would be detrimental to spin injection or detection structures, is possible.¹⁶ Structures should be designed to minimize this process.

We consider four scenarios corresponding to the injection or collection of spin polarized electron current at Schottky contacts to n-type or p-type semiconductors. The four cases are schematically shown in Fig. 1. Panel (a) of Fig. 1 illustrates the case of spin injection into a n-type semiconductor. The diode formed by the Schottky contact is in reverse bias and the electron flux is from the ferromagnetic metal on the left into the semiconductor on the right. A heavily doped region near the interface, as illustrated by the doping profile in the lower part of panel (a), can be designed to form a sharp potential profile through which electrons tunnel. The heavily doped region reduces the effective Schottky energy barrier that determines the properties of the depletion region.¹⁷ The total barrier $e\phi_b$ is divided into two parts, a tunneling region with barrier height $e\phi_t$ and an effective Schottky barrier height eV_{bi} . The potential drop in the depletion region consists of the effective Schottky barrier height plus the applied reverse bias eV_R . Two parameters of the tunneling region, its tunneling resistance and the magnitude of the reduction of the effective Schottky barrier, can be separately controlled by the parameters of the doping profile, for example the height and width of the heavily doped region.

Panel (b) of Fig. 1 illustrates the case of spin-polarization sensitive current detection at a Schottky contact between a ferromagnetic metal and an n-type semiconductor. A spin-polarized electron flux is incident from the semiconductor and the Schottky diode is in forward bias. In a typical experimental situation, the structure is held under constant current bias and a change in voltage signal is sought when the the polarity of the spin-polarized incident current is reversed. There may be a heavily doped region near the interface as in panel (a).

Panel (c) of Fig. 1 illustrates the case of electron spin injection into a p-type semiconductor. The p-type Schottky diode is in strong forward bias. There is an insulating tunneling barrier at the interface that limits the hole current, which nonetheless can be considerable. There is a hole accumulation region in the semiconductor near the interface. The minority carrier electron flux is from the ferromagnetic metal into the semiconductor. This structure can be interesting for characterizing the spin dependent transport properties of the tunneling barrier.

Panel (d) of Fig. 1 illustrates the case of spin-polarization sensitive current detection at a Schottky contact between a ferromagnetic metal and a p-type semiconductor. The p-type Schottky diode is under zero or small (either forward or reverse) bias. Spin polarized electrons are optically generated by absorption of circularly polarized light. In a typical experimental situation, the structure is held under constant current bias and a fixed incident optical intensity and a change

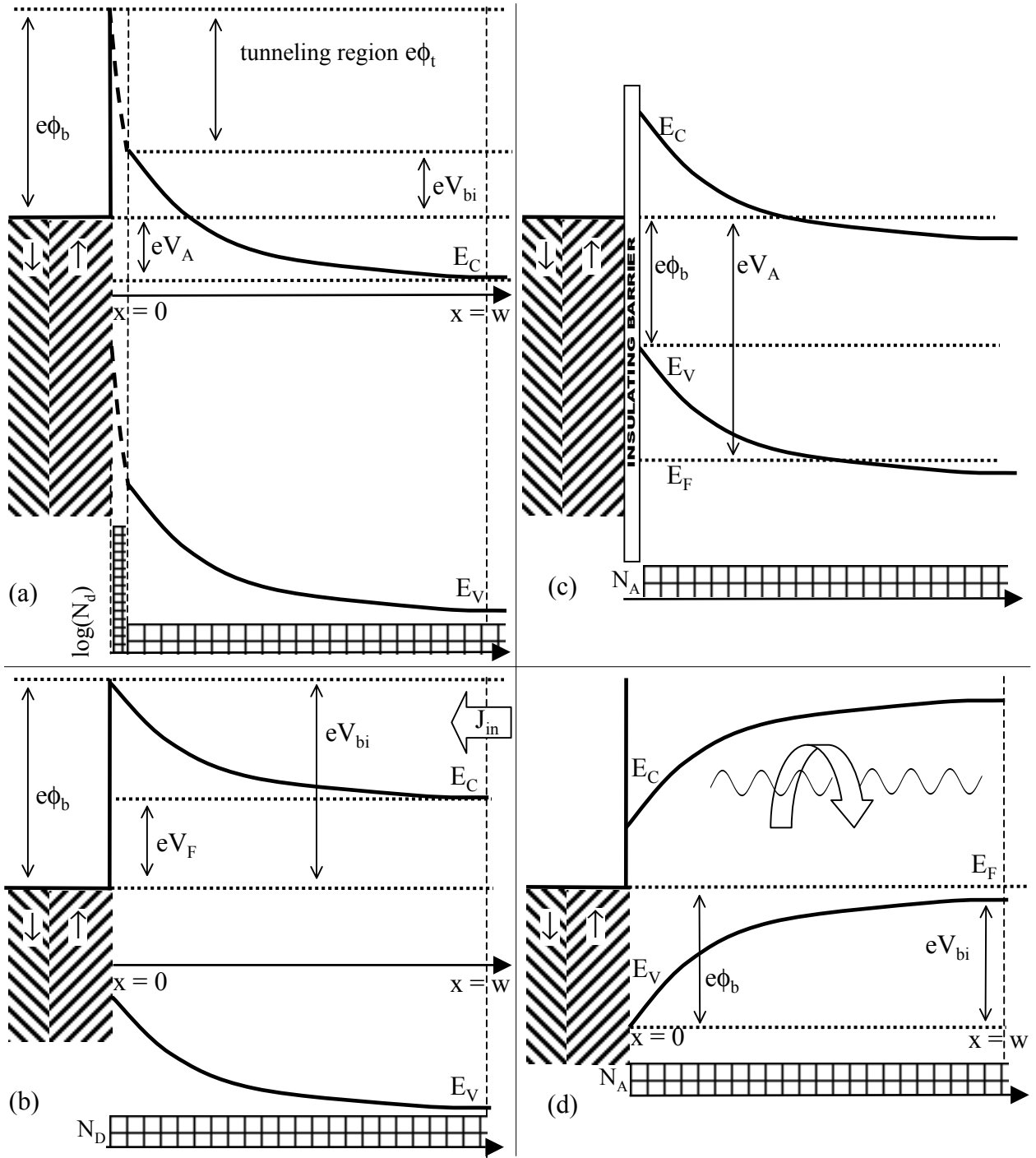


FIG. 1: Energy diagram of a Schottky contact for four cases: (a) electron spin injection into an n-type semiconductor, (b) spin current detection from an n-type semiconductor, (c) spin injection into an accumulated p-type semiconductor, and (d) spin current detection from an optically polarized p-type semiconductor.

in voltage signal is sought when the the polarity of the circularly polarized incident light is reversed. This is the essentially the same structure as in panel (c), except under different bias and optical excitation conditions. These two experimental configurations can be used together to characterize the spin transport properties of a tunneling barrier at the ferro-

magnet/semiconductor interface.

We describe the ferromagnetic metal and the interface using a spin dependent drift-diffusion equation, a spin diffusion equation, and spin dependent interface conductances as in Ref. 4. The drift-diffusion equation describing current flow

in the ferromagnetic metal is

$$j_\eta = \sigma_\eta \frac{\partial (\mu_\eta/e)}{\partial x} \quad (1)$$

Here j_η is the current density due to electrons of spin type $\eta(=\uparrow, \downarrow)$, σ_η is the conductivity for electrons of that spin type, μ_η is the corresponding electro-chemical potential, e is the magnitude of the electron charge and x is position. Eq. (1) assumes rapid wave vector randomizing scattering events, so that electrons of the same spin stay in local quasi-thermal equilibrium with each other. However, spin-flip scattering can be comparatively slow so that electrons of different spin may be driven out of local quasi-thermal equilibrium by, for example, an applied current density. When electrons with different spins are driven out of local quasi-thermal equilibrium, so that μ_\uparrow is not equal to μ_\downarrow at some point in space, spin relaxation away from that spatial point is described by a diffusion equation

$$\frac{\partial^2 \mu_-}{\partial x^2} = \frac{\mu_-}{\Lambda_c^2}. \quad (2)$$

Here Λ_c is the spin diffusion length in the metallic contact and we use the notation $\mu_\pm = \mu_\uparrow \pm \mu_\downarrow$. At the contact/semiconductor interface, electrons of different spin can be driven out of quasi-thermal equilibrium by current flow. Far from the interface, as $x \rightarrow \pm\infty$, the electrochemical potential difference vanishes $\mu_- \rightarrow 0$. The total steady state current density is a constant function of position. We assume no strong spin flip scattering at the interface so that the individual current components for the two spin types are continuous at the interface. Current flow at the interface is described using an interface resistance

$$j_\eta^o = \frac{\Delta\mu_\eta}{eR_\eta} \quad (3)$$

where j_η^o is the current density at the interface, R_η is the interface resistance, and $\Delta\mu_\eta$ is an interfacial discontinuity in electro-chemical potential for electrons of spin type η . If the interface resistance is zero, the electro-chemical potentials are continuous at the interface whereas for nonzero values of R_η a discontinuity in μ_η can develop at the interface. For notational ease, we set the variables $j_\pm = j_\uparrow \pm j_\downarrow$. In the contact where the hole current is zero, the total current $j = j_+$. We take the electron density as a function of position to be fixed, independent of the current density j , in the contact. The total conductivity of the contact is then independent of position and current density. It is convenient to define a contact polarization variable α_c by $\sigma_\uparrow = \alpha_c \sigma_c$ or $\sigma_\downarrow = (1 - \alpha_c) \sigma_c$ where σ_c is the total contact conductivity.

We take the contact on the left ($x < 0$) and the semiconductor on the right ($x > 0$) of the interface located at $x = 0$, as in Fig. 1, so that the current density is negative for electron injection into the semiconductor. Solving Eq. (2) with the stated boundary conditions gives

$$\mu_- = \mu_-^{0-} e^{x/\Lambda_c} \quad \text{for } x < 0. \quad (4)$$

Quantities evaluated at the interface approached from the contact and semiconductor are indicated by the superscripts 0^- and 0^+ , respectively. From Eqs. (1) and (4) we find

$$\begin{aligned} \mu_-^{0-} &= e\Lambda_c \left(\frac{j_\uparrow^{0-}}{\sigma_\uparrow} - \frac{j_\downarrow^{0-}}{\sigma_\downarrow} \right) \\ &= \frac{e\Lambda_c}{2\sigma_c\alpha_c(1-\alpha_c)} \left(j_+^{0-} + j_-^{0-} - 2\alpha_c j_+^{0-} \right), \end{aligned} \quad (5)$$

and

$$\frac{\partial \mu_+}{\partial x} = \frac{2ej}{\sigma_c} + \frac{(1-2\alpha_c)}{\Lambda_c} \mu_-^{0-} e^{x/\Lambda_c}. \quad (6)$$

The total current in the semiconductor is $j = j_\uparrow + j_\downarrow + j_p = j_+ + j_p$ where j_p is the hole current density. For n-type Schottky barriers $j_p = 0$, but not necessarily for the p-type structures. It is convenient to define β as the fraction of the electron current carried by spin up electrons $\beta = j_\uparrow / j_+$. We assume that there is not strong spin-flip scattering at the interface so that $j_-^{0-} = j_-^{0+}$. The total current j is continuous at the interface. The interface resistance conditions, Eq. (3) then lead to the interface matching conditions,

$$\begin{aligned} \mu_-^{0-} &= \frac{e j_+^{0+} \Lambda_c}{\sigma_c \alpha_c (1 - \alpha_c)} \\ &\times \left[\beta^{0+} - \alpha_c - \left(\alpha_c - \frac{1}{2} \right) \frac{(j - j_+^{0+})}{j_+^{0+}} \right] \end{aligned} \quad (7)$$

$$\mu_-^{0+} - \mu_-^{0-} = e j_+^{0+} \left(\beta^{0+} (R_\uparrow + R_\downarrow) - R_\downarrow \right) \quad (8)$$

$$\mu_+^{0+} - \mu_+^{0-} = j \left(\beta^{0+} (R_\uparrow - R_\downarrow) + R_\downarrow \right). \quad (9)$$

These matching conditions apply for each of the four cases illustrated in Fig. (1).

The semiconductor near the interface is either depleted, as shown in panels (a), (b) and (d) in Fig. 1, or accumulated as shown in panel (c) in Fig. 1. We input the drop in electrostatic potential between the semiconductor side of the interface and the edge of the depletion or accumulation region. A tunneling region, such as is illustrated in panel (a) in Fig. 1 is described by the interface resistances R_\uparrow and R_\downarrow , and is taken to have negligible width. The semiconductor side of the interface starts at the right of the tunneling region. From the input potential drop we calculate: the current density; the net bias voltage, which may include a contribution from the interface resistance; and the electrostatic profile. For the depleted cases we use the usual depletion approximation to describe the electrostatics in the semiconductor. For the accumulated case, we assume that hole current is limited by an interfacial barrier, take a constant hole quasi-Fermi energy in the semiconductor as shown in Fig. 1(c), and solve Poisson's equation self-consistently to determine the electrostatic potential

in the accumulation region. Details of the electrostatics are described in Appendix A.

In the semiconductor, electron and hole currents satisfy continuity equations,

$$\frac{\partial j_\eta}{\partial x} = -e(g_\eta - r_\eta), \quad (10)$$

and

$$\frac{\partial j_p}{\partial x} = e(g_p - r_p), \quad (11)$$

where g is a generation rate and r a recombination rate. For spin polarized electrons there is a contribution to the recombination rate from both spin flip scattering and electron-hole recombination,

$$r_\uparrow = \frac{n_\uparrow}{\tau_r} + \frac{n_\uparrow - n_\downarrow}{\tau_s}, \quad (12)$$

where τ_r and τ_s are the recombination and spin flip times, respectively, and an analogous expression applies for r_\downarrow . We use a drift-diffusion approximation to describe electron and hole currents,

$$j_\eta = \bar{\mu}_n \frac{n_i}{2} kT e^{e\phi/kT} \frac{\partial e^{\mu_\eta/kT}}{\partial x}, \quad (13)$$

and

$$j_p = -\bar{\mu}_p n_i kT e^{e\phi/kT} \frac{\partial e^{-\mu_p/kT}}{\partial x} \quad (14)$$

where $\bar{\mu}_{n(p)}$ is the electron (hole) mobility, n_i is the intrinsic carrier concentration and ϕ is the electrostatic potential. The carrier densities are given by

$$n_\eta = \frac{n_i}{2} e^{(e\phi + \mu_\eta)/kT} \quad (15)$$

and

$$p = n_i e^{-(e\phi + \mu_p)/kT}. \quad (16)$$

It is convenient to go into a representation describing the electron charge and spin degrees of freedom and we define

$$\Omega_\pm = e^{\mu_\uparrow/kT} \pm e^{\mu_\downarrow/kT}. \quad (17)$$

so that

$$j_\pm = \bar{\mu}_n \frac{n_i}{2} kT e^{e\phi/kT} \frac{\partial \Omega_\pm}{\partial x}, \quad (18)$$

and

$$n_\pm = \frac{n_i}{2} e^{e\phi/kT} \Omega_\pm. \quad (19)$$

The corresponding generation and recombination rates are $g_\pm = g_\uparrow \pm g_\downarrow$, $r_+ = n_+/\tau_r$, and $r_- = n_-(2/\tau_s + 1/\tau_r)$. The continuity equations become

$$\frac{\partial j_\pm}{\partial x} = -e(g_\pm - r_\pm). \quad (20)$$

Substituting the drift-diffusion form into the continuity equation gives a transport equation for Ω_\pm ,

$$\frac{\partial^2 \Omega_\pm}{\partial x^2} + \left(\frac{e}{kT} \frac{\partial \phi}{\partial x} \right) \frac{\partial \Omega_\pm}{\partial x} - \frac{1}{\Lambda_\pm^2} \Omega_\pm = -e\tilde{g}_\pm e^{-e\phi/kT} \quad (21)$$

where $\tilde{g}_\pm = g_\pm / [\bar{\mu}_n (kT/e)(n_i/2)]$, $\Lambda_\pm^2 = (kT/e)\bar{\mu}_n \tau_r$, and $\Lambda_-^2 = (kT/e)\bar{\mu}_n (2/\tau_s + 1/\tau_r)^{-1}$. An analogous equation holds for holes. Analytic solutions for Ω_\pm are discussed in Appendix B.

Boundary conditions at the semiconductor side of the interface, $x=0^+$, and at the depletion edge, $x=w$, are used to determine the two matching coefficients (see Appendix B) that appear in the solutions of Eq. (21). Details of the boundary conditions differ somewhat for the individual cases and will be specified in the discussion of these cases. For the charge degree of freedom, we use interface recombination boundary conditions at the semiconductor side of the interface,

$$j_+^{0+} = ev_{sr} \left(n_+^{0+} - n_{eq}^{0+} \right) \quad (22)$$

where v_{sr} is the surface recombination velocity and n_{eq}^{0+} is the equilibrium electron density at the semiconductor side of the interface. For the n-type semiconductor cases we set the electron density at the depletion edge ($x=w$) equal to the bulk doping density so that that the material becomes charge neutral at this point $n_+(w) = N_d$ where N_d is the bulk doping density. From the definition of Ω_\pm , we see that

$$\mu_- = 2kT \tanh^{-1} \left(\frac{\Omega_-}{\Omega_+} \right). \quad (23)$$

Combined with Eq. (7) this gives a boundary condition for Ω_- at the semiconductor side of the interface. It is often useful to write

$$\frac{\Omega_-}{\Omega_+} = \frac{\frac{\partial \ln \Omega_+}{\partial x}}{\frac{\partial \ln \Omega_-}{\partial x}} (2\beta - 1) \quad (24)$$

and

$$(2\beta - 1) = \frac{j_-}{j_+} = \frac{\frac{\partial \Omega_-}{\partial x}}{\frac{\partial \Omega_+}{\partial x}}. \quad (25)$$

This form can be useful because $(2\beta - 1)$ can become the unknown in the matching condition of Eq. (8). In the doped material beyond the depletion region the electric field is small and spatially uniform. In the usual treatment of current flow in Schottky diodes this small field is neglected. For most of the cases there is no generation term in Eq. (21) and we only need the homogenous solution for Ω_-

$$\Omega_-(x \geq w) = \Omega_-(w) \exp[(w - x)/\ell_+] \quad (26)$$

where

$$\ell_\pm^{-1} = \pm \frac{e|E|}{2kT} + \sqrt{\left(\frac{e|E|}{2kT} \right)^2 + \left(\frac{1}{\Lambda_s} \right)^2}. \quad (27)$$

Here, E is the uniform electric field in the doped material beyond the depletion region. Substituting into Eq. (19) we obtain the more familiar notation of the “drift-diffusion” framework. In the bulk, n_- relaxes according to

$$n_-(x \geq w) = n_-(w) \exp[(w - x)/\ell_-] \quad (28)$$

where ℓ_- reflects the field modification of the diffusion length at constant carrier density.²⁷ Matching the continuity of Ω_- and its spatial derivative, the current from Eq. (1), at the edge of the depletion region give the final boundary conditions.

III. CALCULATED RESULTS OF MODEL CONTACTS

We discuss results for each of the four cases shown in Fig. 1 sequentially.

A. Injection at an n-type contact.

This section discusses results for electron spin injection at an n-type Schottky contact as shown in Fig. 1(a). The effective Schottky barrier of the contact can be varied by changing the doping profile in the semiconductor near the interface as shown at the bottom of the panel. We consider a heavily doped region near the interface that creates a narrow tunneling region. The effect of the narrow doping region is to reduce the effective Schottky barrier energy with the associated reduction in the depletion width. This approach to tailoring effective Schottky barriers is well established in semiconductor device applications.¹⁷

For this case, there is no hole current or optical generation. Consequently, we solve the homogeneous form of Eq. (21) matched to boundary conditions at the interface given by Eqs. (7-9) and at the depletion edge by Eqs. (26) and (1). The tunneling regions are parameterized using interface resistances and reduced effective Schottky barriers. The contact is metallic with resistance equal to $10^{-5} \Omega \text{ cm}$, polarization $\alpha_c = 0.9$ (80% polarized) and spin diffusion length equal to $\Lambda_c = 100 \text{ nm}$. The n-type semiconductor has an electron mobility of $\bar{\mu}_n = 5000 \text{ cm}^2/(\text{V s})$ and a spin diffusion length equal to $1.0 \mu\text{m}$. The diode characteristic from Eq. (22) is determined using $v_{sr} = 10^7 \text{ cm/s}$.

In Figs. 2, 3, and 4 we show calculations of spin injection through a depleted n-type Schottky contact at $T = 300 \text{ K}$. In Fig. 2, we show the effect of the effective Schottky barrier on spin injection. In panel (a), the current spin polarization as a function of position is plotted for three effective Schottky energy barriers, as labelled in the figure. For each barrier energy, the structure is biased to operate at 90% of the reverse-saturation current. The calculation shows clearly that the presence of an energy barrier degrades the performance of the spin injecting structure, and that the dependence on barrier height is strong. In panel (b), the corresponding electrochemical potential differences are plotted for each structure. We see from this panel that the origin of the splitting in electrochemical potentials (directly related to polarization) is from the interface resistance.

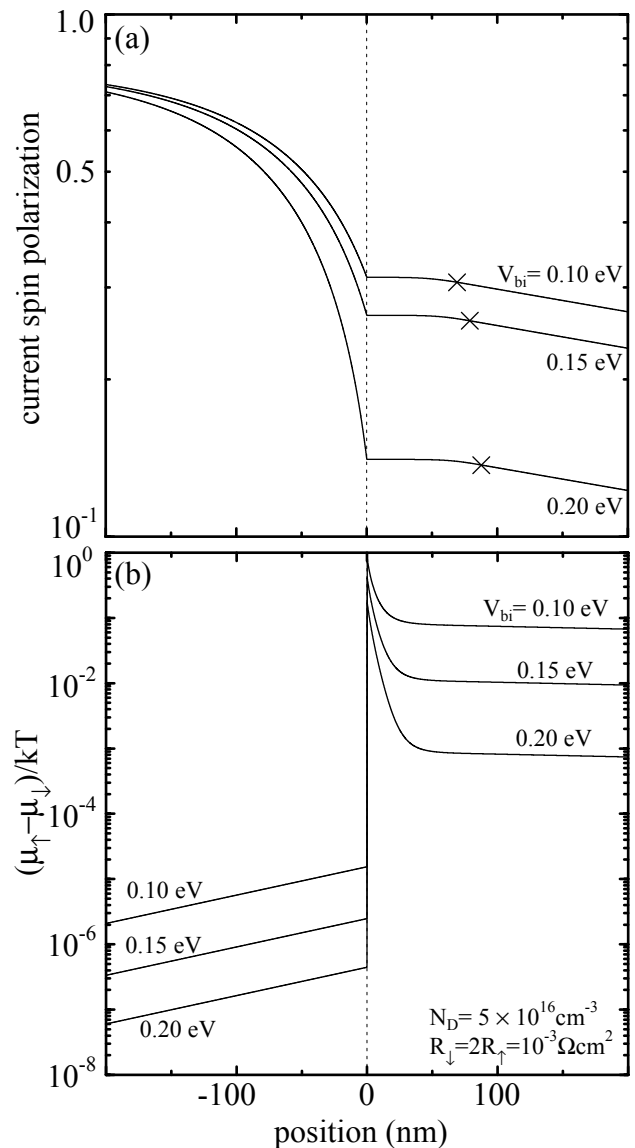


FIG. 2: Calculated spin injection properties for an n-type Schottky contact as shown in Fig. 1(a). (a) Current spin polarization (j_-/j_+); and (b) electrochemical potential difference for spin-up and spin-down electrons as a function of position for various values of the effective Schottky barrier. The edge of the depletion region is indicated by \times on the curves of part (a).

If the interface resistance is lowered or if the R_\uparrow/R_\downarrow ratio approaches unity, then the injection properties of the structure degrade. Some specifics regarding the barrier lowering and interface resistance for the n-type injector are discussed Ref. 8.

The electron spin density polarization can be examined in the presence of the electron density profile. For the same conditions used in Figs. 2, the spin polarization of the local electron density is shown in panel (a) of Fig. 3. The total density is shown in panel (b) of Fig. 3 for comparison. The polarized current may persist deeper into the semiconductor than its ability to spin polarize the local electron gas. A spin polar-

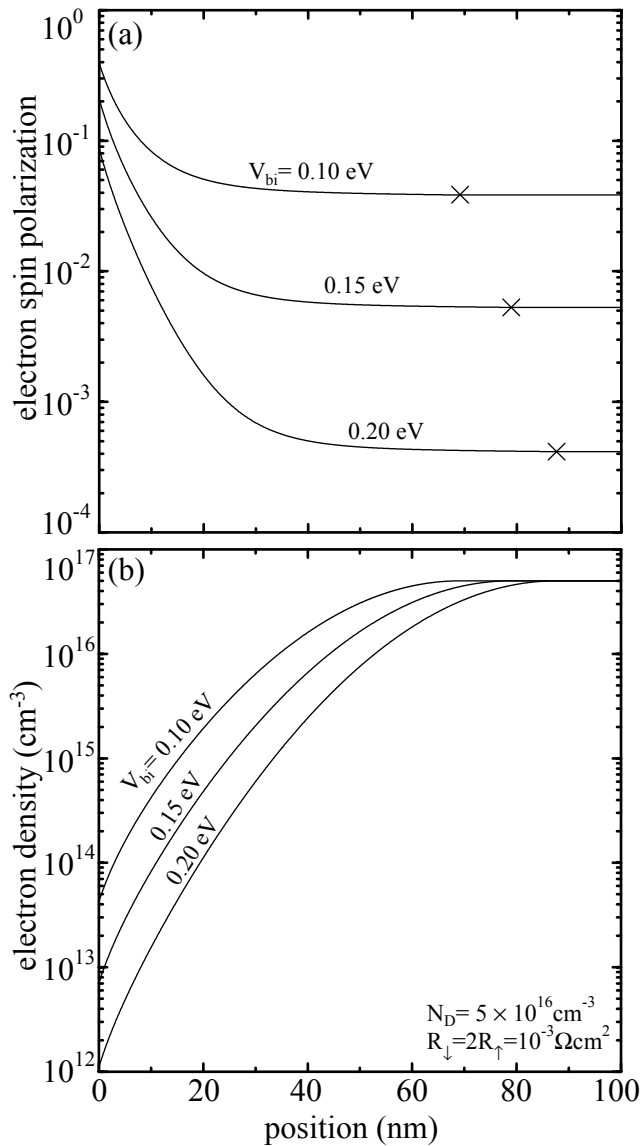


FIG. 3: Effect on the local spin populations of injection at an n-type contact as shown in Fig. 1(a). (a) Electron density spin polarization (n_-/n_+); and (b) total electron density (n_+) as a function of position for various values of the effective Schottky barrier. The edge of the depletion region is indicated by the \times on the curves of part (a).

ized current may be established in the semiconductor without strongly perturbing the spin polarization of a background of free carriers. However, for optical detection, such as the spin-LED, the signal is proportional to the spin polarization of the local density and not of the current.

In the calculations presented in Fig. 2 and Fig. 3 the effect of an electric field in the doped region outside the depletion region was neglected. This is the usual approximation in describing the electrical properties of Schottky diodes. It is reasonable because the doped region outside the depletion region is conductive and the current flow is limited by the depletion region. In Fig. 4 we compare a calculation of the current polarization as a function of position neglecting the electric field

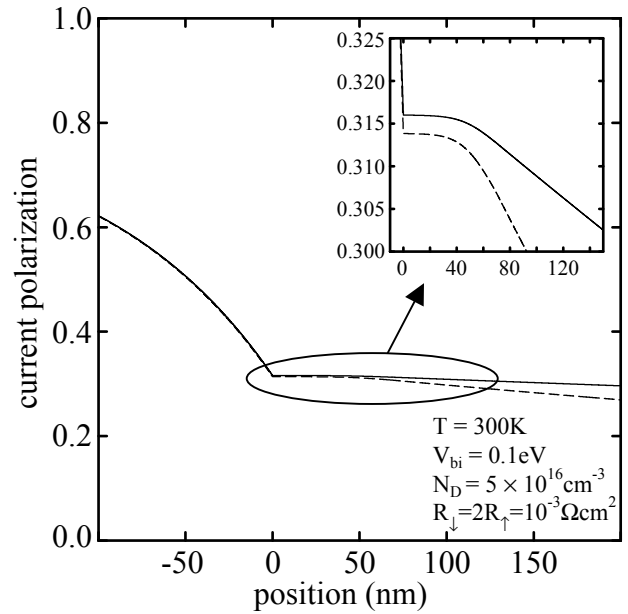


FIG. 4: Effect of an electric field beyond the depletion region. The solid curve shows current polarization as a function of position including a greatly exaggerated electric field in the doped region beyond the depletion region whereas the dashed curve assumes no electric field outside the depletion region (as in Fig. 2) for $V_{bi} = 0.1\text{V}$. The field used for the solid line was chosen to give $\ell_- = 10\mu\text{m}$, or 70 times the value determined from drift in the bulk. If the field determined by $en_+\bar{\mu}_n$ and j is used, the result is essentially indistinguishable from that using zero field.

in the doped region with one which includes a greatly exaggerated value for the electric field outside the depletion region for an effective barrier height of 0.1 eV. The field used for the solid line was chosen to give $\ell_- = 10\mu\text{m}$ and is 70 times that determined by the conductance of this region and the injected current density. If a field determined by the conductance and current density ($E = j/en_+\bar{\mu}$) is used, the result is essentially indistinguishable from that using zero field. (For the calculation in Fig. 4 that field is -37 V/cm.) The figure shows that for a Schottky structure with a significant effective barrier height the electric field in the doped region outside the depletion region has little effect on the spin injection properties of the structure. The reason for this is that the matching conditions on the currents and electrochemical potentials are at the interface between the metal and the depleted region of the semiconductor where the concentration of electrons is exceedingly small. This is to be contrasted with uniform conductivity models where the electron concentration is the same up to the interface so that $\partial\mu_n/\partial x$ is driven by the electric field on the semiconductor side.^{2,7}

The depleted region that occurs at a Schottky contact is seen to be detrimental to spin injection at a ferromagnetic metal/ semiconductor interface. The problem arises because injection is into a very low resistance region of the semiconductor that is depleted of carriers. However, the depletion region can be tailored using a doping density profile to minimize these deleterious effects. For example, a heavily doped region

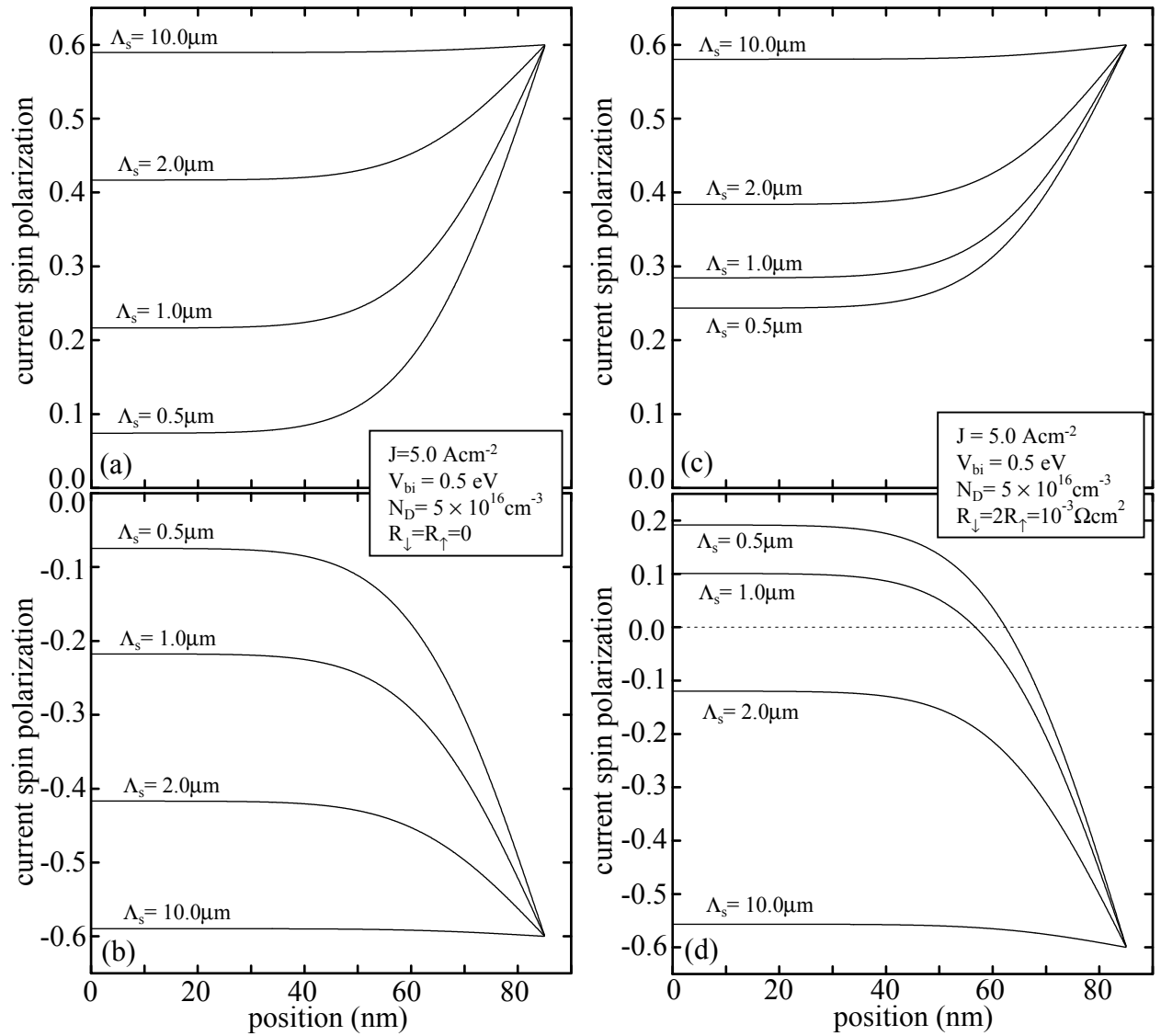


FIG. 5: Current spin polarization in the semiconductor for an n-type Schottky structure operating in detection mode as shown in Fig. 1(b). Results are plotted for various Λ_s at fixed V_{bi} . The electron flux, incident right-to-left at the depletion edge, corresponds to a current equal to 5.0 A cm^{-2} . (a) Incident polarization $j_-(w)/j_+=0.6$ and zero interface resistance. (b) $j_-(w)/j_+=-0.6$ and zero interface resistance. (c) $j_-(w)/j_+=0.6$ with fixed interface resistance. (d) $j_-(w)/j_+=-0.6$ with fixed interface resistance.

near the interface, such as a delta-doped layer, can be used to form a sharp potential profile through which electrons tunnel to reduce the effective Schottky energy barrier that determines the magnitude of the depletion region.

B. Detection at an n-type contact.

This section describes results for spin detection at n-type Schottky structures as shown in Fig. 1(b). The spin detection case is similar to that of spin injection discussed in the previous section but with a modification of the boundary conditions. The boundary condition on the current spin polarization at $x=w$ is an incident polarized current $j_-(w)$. We consider a constant total current density of 5.0 A cm^{-2} and seek a volt-

age signal as the polarity of the spin polarization is reversed. The contact is metallic and has the same properties as in the previous section.

The calculated current polarization as a function of position within the depletion region for detector operation is shown in Figs. 5 and 6. Results are calculated for 60% incident spin polarization. In Fig. 5, we examine the dependence of the spin polarized current on Λ_s for fixed effective Schottky barrier. Since the effective Schottky barrier is fixed the depletion width is the same for the various cases. Long spin relaxation times result in larger spin polarizations at the interface. In panels (a) and (b) of Fig. 5 the current polarization behavior is almost identical for up and down incident currents when the interface resistance is zero. This shows that the presence of a polarized contact material (polarized spin up) has little impact

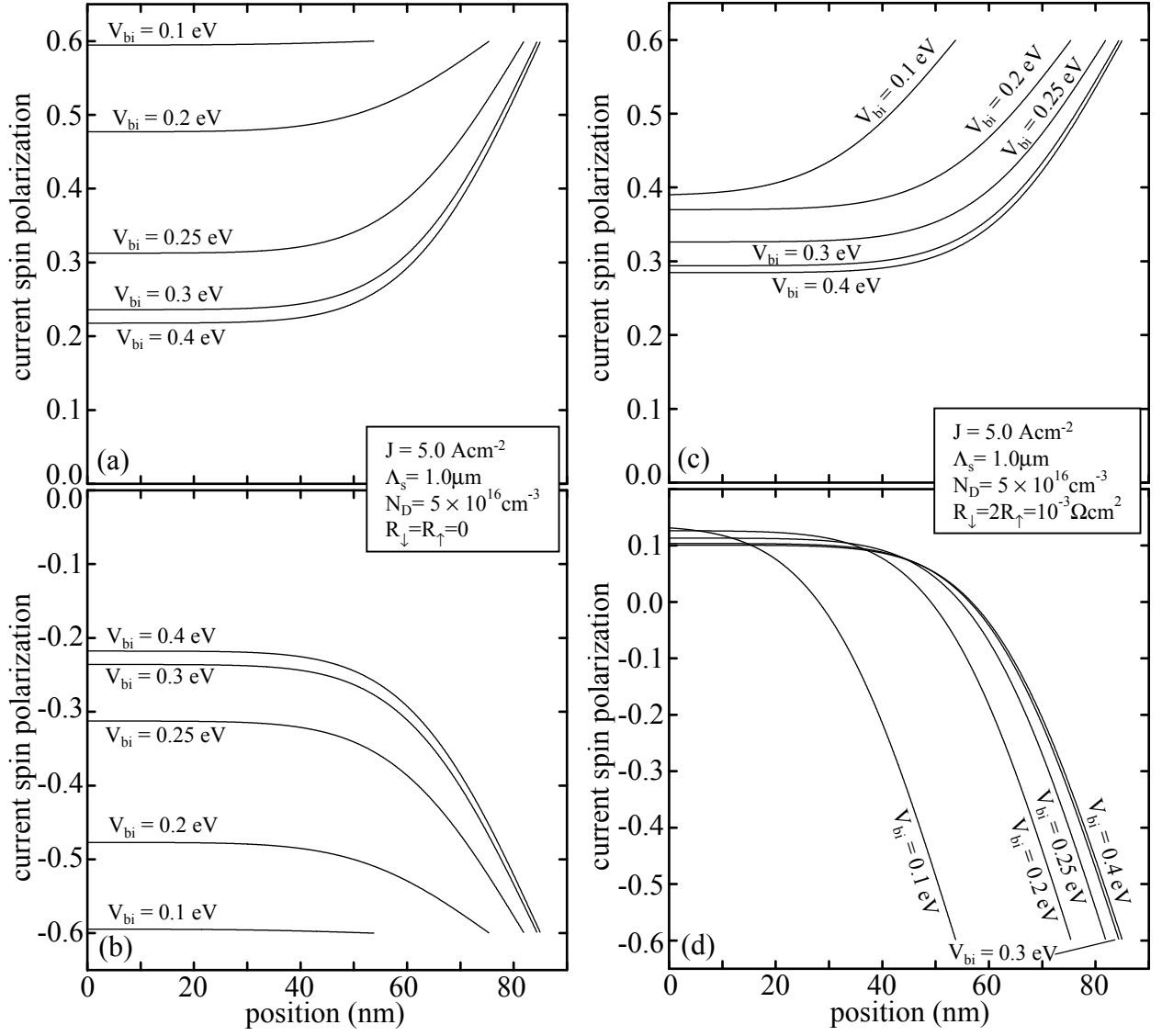


FIG. 6: Current spin polarization in the semiconductor for an n-type Schottky structure operating in detection mode as shown in Fig. 1(b). Results are plotted for various V_{bi} at fixed Λ_s . The electron flux, incident right-to-left at the depletion edge, corresponds to a current equal to 5.0 A cm^{-2} . (a) Incident polarization $j_-(w)/j_+=0.6$ and zero interface resistance. (b) $j_-(w)/j_+=-0.6$ and zero interface resistance. (c) $j_-(w)/j_+=0.6$ with fixed interface resistance. (d) $j_-(w)/j_+=-0.6$ with fixed interface resistance.

on the spin polarized current in the semiconductor. In panels (c) and (d) the currents are calculated including interface resistance and show a strong asymmetry owing to the mismatch in R_\uparrow and R_\downarrow .

In Fig. 6 we examine the dependence of the current polarization in the depletion region on V_{bi} at fixed Λ_s . The bias conditions have been adjusted to give the same total current density for all cases. Structures with different barrier heights have different depletion widths. A main point seen from Fig. 6 is that large effective barrier energies result in small spin polarizations at the interface. In panels (a) and (b) of Fig. 6 the current polarization behavior is very close for up and down incident currents when the interface resistance is zero. In panels (c) and (d) the currents are calculated including interface resistance and show a strong asymmetry owing to the mismatch

in R_\uparrow and R_\downarrow .

We consider an n-type Schottky detector structure at a constant total current density. To fix the total current in the structure, the forward bias (V_F in Fig. 1(b)) is tuned for each structure. The detected signal is the change in voltage at fixed current density when the spin polarization of the incident current is reversed. This voltage difference is obtained by integrating the electrochemical potential over position from $-\infty$ to $+\infty$ and taking the difference for two incident spin polarizations. After cancellations, the surviving terms yield a voltage difference of

$$\Delta V = \Delta \left(\frac{j_-^{0+}}{j_+} \right) \times \frac{j_+}{4} \left[R_\uparrow - R_\downarrow + \frac{\Lambda_c (1 - 2\alpha_c)}{\sigma_c \alpha_c (1 - \alpha_c)} \right] \quad (29)$$

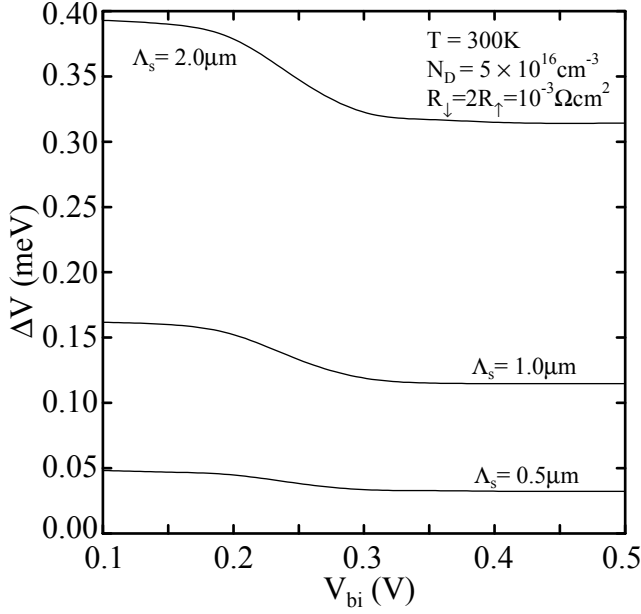


FIG. 7: Voltage signal as a function of effective Schottky barrier energy for $j_-/j_+ = \pm 0.6$ and incident current equal to 5.0 A cm^{-2} . Results are shown for three values of the spin diffusion length.

where Δ indicates the difference between the quantities for opposite signs of the incident spin polarization at $x=w$.

From Eq. (29) we see that without a spin dependent interface resistance ($R_\uparrow = R_\downarrow \rightarrow 0$) and for a highly conductive contact ($\sigma_c \rightarrow \infty$) no significant voltage difference can be established. Using metallic contacts ($\sigma_c = 10^5 \text{ } \Omega \text{ cm}^{-1}$) with contact spin diffusion lengths less than a micron ($\Lambda_c = 10^{-5} \text{ cm}$) and currents ($\sim 1 \text{ A cm}^{-2}$) corresponding to low biasing conditions the calculated detected voltage differences are negligibly small ($\lesssim 10^{-10} \text{ V}$). We conclude that Schottky contacts without a spin-selective tunnel barrier will not be useful as spin polarized current detectors and therefore we concentrate on Schottky structures containing a spin selective interface resistance. In Fig. 7 we show calculated voltage differences as a function of effective Schottky barrier for three values of the spin-diffusion length in the semiconductor. The detection signal saturates for both large and small V_{bi} values. For small barriers the depletion region vanishes and the incident polarized current reaches the interface and only small applied bias is required to establish the constant current. For large depletion widths, larger applied biases are required to keep the current density fixed and the resulting interface current polarization saturates consistent with the behavior shown in Fig. 6(c) and 6(d).

The depleted region that occurs at a Schottky contact is seen to be detrimental to spin detection at a ferromagnetic metal/ semiconductor interface. The problem arises because in these forward biased structures, electron current is driven by diffusion against a strong and rapidly varying electric field in the depletion region. As a result the effective drift-diffusion lengths in the depletion region can become rather short leading to strong spin relaxation. As for the electron injection

structures the depletion region can be tailored using a doping density profile to minimize these deleterious effects.

C. Injection at a p-type contact.

This section describes results for spin polarized electron injection from a ferromagnetic contact into a forward biased p-type Schottky diode. The hole current is limited by a barrier at the interface but is most likely larger than the minority electron injection current. The output signal is the ratio of right to left circularly polarized light emitted from the semiconductor when the injected electrons recombine radiatively with unpolarized holes in the p-type material.

The electrostatic treatment for the p-type structure is de-

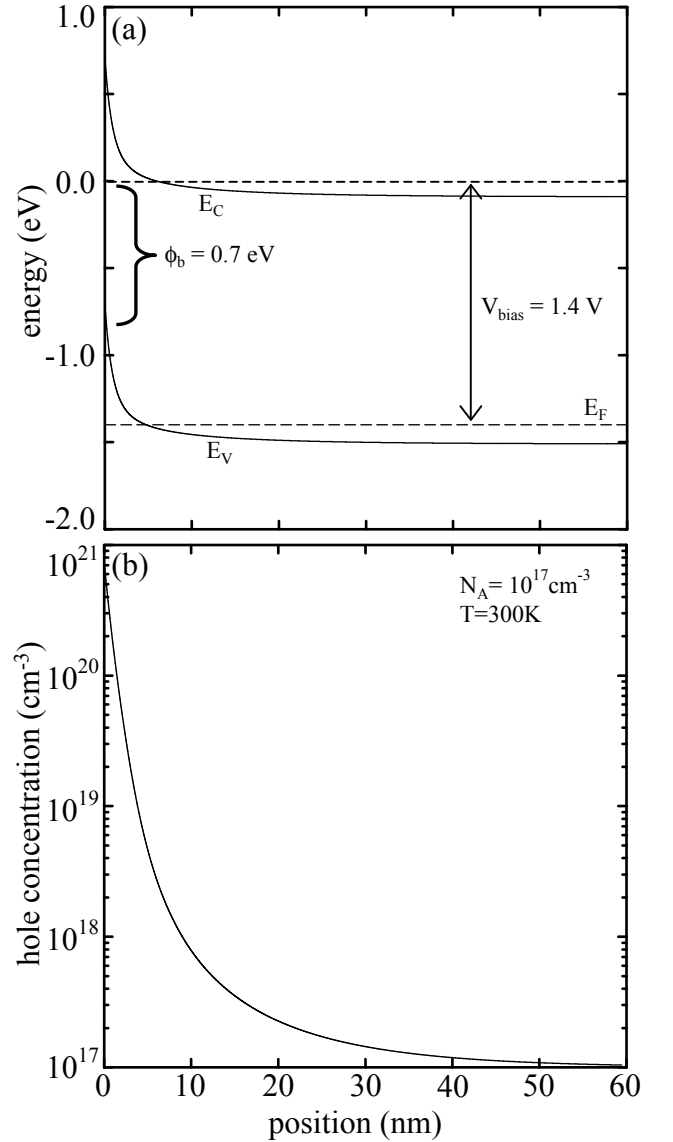


FIG. 8: Energy band diagram (a) and hole density profile (b) of an accumulated p-type Schottky diode in strong forward bias as in Fig. 1(c).

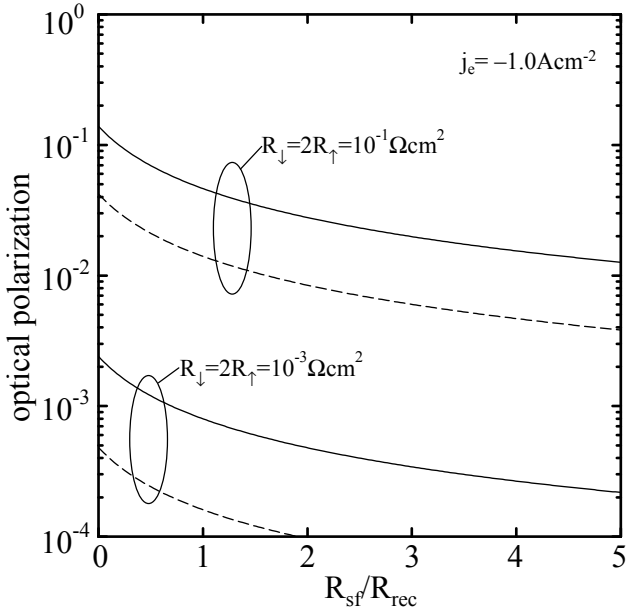


FIG. 9: Integrated emitted photon polarization $(\sigma_+ - \sigma_-)/(\sigma_+ + \sigma_-)$ as a function of electron spin-flip scattering rate coefficient for fixed injected current density from a ferromagnetic contact ($\alpha_c=0.9$) into the accumulated p-type contact shown in Fig. 8. Results are shown for injection efficiencies of $j_+/j=0.5$ (solid curves) and 0.1 (dashed curves).

scribed in Appendix A. Calculated energy band and hole concentration profiles are shown in Fig. 8 and correspond to the semiconductor portion of Fig. 1(c). An interfacial barrier is an important feature of the structure to prevent runaway hole current at the interface. As a consequence of the barrier there is strong accumulation of holes near the interface. The large and rapidly varying hole concentration requires a different treatment of the electron spin relaxation process¹⁸ than used in the depletion cases considered above. To account for the presence of the accumulated holes, we use the local hole concentration to vary the recombination and spin-flip scattering rates as a function of position.

We take the electron spin relaxation times to be linear with the local hole density and define rate coefficients R_{sf} and R_{rec} for spin-flip scattering and recombination so that $\tau_s^{-1} = R_{sf} \times p(x)$ and $\tau_r^{-1} = R_{rec} \times p(x)$. We present calculations for a range of R_{sf} . We take $R_{rec} = 7 \times 10^{-10} \text{ cm}^3 \text{ s}^{-1}$, a typical value for p-type GaAs at $T=300\text{K}$.¹⁹ The hole mobility is $\mu_p = 500 \text{ cm}^2/(\text{V s})$.

Unlike for the depleted structures there is no closed form analytic solution for the spin-dependent transport equations for the accumulated structure. Given a numerical solution for $p(x)$ from the electrostatic calculation, the solution of Eq. (21) is obtained by numerical integration and the shooting criterion that solutions be non-diverging as $x \rightarrow \infty$. There is no optical generation of carriers ($g_{\pm}=0$) so that only the homogeneous solution is required.

The detected quantity in this case is the degree of circular polarization of the emitted light. Assuming good radiative recombination efficiency, the optical polarization of right and

left circularly polarized light (σ_{\pm}) is proportional to the local electron density and is given by

$$\frac{\sigma_+ - \sigma_-}{\sigma_+ + \sigma_-} = \frac{\int_0^{\infty} n_- dx}{\int_0^{\infty} n_+ dx} = \frac{\Lambda_-^2}{\Lambda_+^2} (2\beta^{0+} - 1). \quad (30)$$

The spin polarization ($2\beta^{0+} - 1$) of the electron current at the interface is obtained from the numerical solution of Eq. 21. The integration is straightforward because the electron concentrations are related to the current through the continuity equations, Eqs. (10-12).

The calculated optical polarizations for injection into p-type material are shown in Fig. 9 as a function of the spin-flip scattering rate coefficient. The curves are calculated for the same electron current density at $x=0$. We consider insulating barriers that result in minority carrier injection efficiencies equal to 50% and 10%. If used as a characterization tool, the structure should be sensitive to differences in the optical polarization signals in order to determine the interface resistance values. This is the case for the case of slow spin-flip scattering compared radiative recombination. If the spin-flip scattering rate is faster than the recombination rate in the semiconductor characterization by this method is will to be difficult.

D. Detection at a p-type contact.

The p-type detector structure shown in Fig. 1(d) involves optical generation of carriers. The p-type Schottky diode is at zero or small bias (either forward or reverse). As in the depleted n-type detector, we compute the voltage difference established as the circular polarization of the light is changed

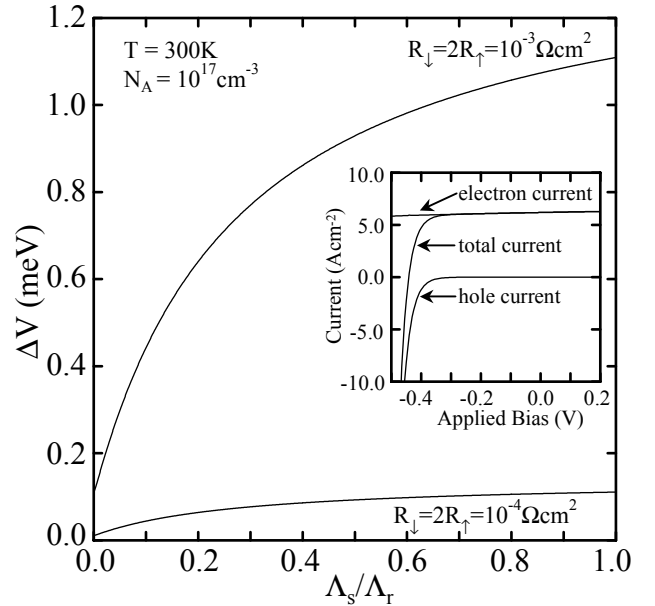


FIG. 10: Voltage difference for collection of spin polarized electrons at a depleted p-type contact. The inset shows the electron and hole current contributions to the current-voltage characteristics.

from right to left. We assume that the optical generation is nearly uniform over the depletion depth (i.e., that the reciprocal of the absorption coefficient is small compared to the depletion width) and that the optical generation of spin-polarized carriers is a 3:1 or 1:3 ratio of spin-up to spin-down electrons according to the optical selection rules. Beyond the depletion edge, for $x > w$, the optical generation falls off as $\exp(-\chi x)$ with $\chi = 10^4$ cm. Under these conditions, the transport equation (21) is solved analytically as described in Appendix B.

A calculated current/voltage characteristic for the various current components calculated for this structure are shown in the inset of Fig. 10. The properties of the p-type Schottky are those used in the accumulation case of the previous section. The barrier height is 0.7eV and the incident light power is set to 1 W cm^{-2} or $g_+ \approx 4.4 \times 10^{22} \text{ s}^{-1} \text{ cm}^{-3}$ for photons at the bandgap of GaAs. In this structure, the electron current stays nearly constant over a broad range of applied bias around $V_A = 0$ so we report results for zero bias. The value for ΔV , as for the n-type detector structure, is given by Eq. (29) except that the total electron current at the interface j_+ must be accounted for separately from the total current which includes a contribution from holes. This separation is straightforward once solutions for $\Omega_{\pm,p}$ have been calculated. In Fig. 10 we plot the calculated voltage differences as a function of Λ_s for optical excitation. If the semiconductor spin lifetime has been determined by other experimental means, this represents a second method of characterizing the interface resistance. Notice that even when the spin lifetime becomes maximally long ($\Lambda_s = \Lambda_r$) there is a strong dependence of the measured voltage on the interfacial conditions.

IV. SUMMARY

We have presented a theoretical description of the injection and detection of spin polarized electrons at n-type and p-type Schottky contacts. The presence of the depletion region that occurs at Schottky contacts has been shown to be detrimental to both spin injection and detection in n-type Schottky structures. The problem for the reverse biased n-type spin injection structures arises because the injection is into a very low resistance region of the semiconductor that is depleted of carriers. The problem for the forward biased n-type spin detection structures arises because electron current is driven by diffusion against a strong and rapidly varying electric field in the depletion region. As a result the effective drift-diffusion lengths in the depletion region can become rather short leading to strong spin relaxation in the depletion region.

For both n-type injection and detection structures, the depletion region can be tailored using a doping density profile to minimize these deleterious effects. A heavily doped region near the interface, such as a delta-doped layer, can be used to form a sharp potential profile and this tunneling region effectively reduces the Schottky energy barrier that determines the magnitude of the depletion region. The model results indicate that efficient spin-injection and spin-polarization detection can be achieved in these n-type structures if they are properly designed so that the effective Schottky barrier is reduced

to less than about 0.2 eV.

We discussed two experimental cases in which ferromagnetic Schottky contacts to p-type semiconductors could be used to characterize the spin dependent transport properties of interface tunnel barriers: optical detection of spin currents injected into a strongly forward biased accumulated p-type semiconductor and electrical measurement of optically excited spin populations at zero biased p-type contacts. The same structure can be used under different bias and excitation conditions for the two experiments.

A set of spin-labelled transport equations has been developed, in a systematic way, that is suitable for device models at a basic level. We have demonstrated that the electrostatic and current conditions that are present in actual devices can lead to important consequences for spin dependent transport in the structures must be taken into account. With these building blocks in place, there are clear extensions of the model to more complex device structures which will be the focus of future work.

Acknowledgments

This work was supported by the SPINs program of the Defense Advance Research Projects Agency.

APPENDIX A: SCHOTTKY CONTACT ELECTROSTATICS

The band-bending that occurs near a Schottky contact is central to the discussion of spin transport in these structures. This appendix describes the electrostatic inputs to the solutions of the spin transport equations.

Three of the cases, shown in Fig. 1(a), (b), and (d), involve a contact under small bias. In these cases, we use the depletion approximation where the electrostatic potential and depletion width are given by

$$\phi(x) = \phi(0) \pm \frac{eN}{\epsilon_s \epsilon_o} wx \mp \frac{1}{2} \frac{eN}{\epsilon_s \epsilon_o} x^2 \quad 0 \leq x \leq w \quad (\text{A1})$$

and

$$w = \sqrt{\frac{2\epsilon_s \epsilon_o}{eN} (V_{bi} + V_A)} \quad (\text{A2})$$

here ϵ_o is the free space permittivity, and ϵ_s is the relative static dielectric constant of the semiconductor. The applied voltage V_A can be either sign but must be small enough in forward bias so as not to invert the semiconductor from depletion to accumulation. For an n-type contact, N is the donor concentration and the upper sign applies. The acceptor concentration and the lower sign are used for p-type contacts.

The inverted p-type contact shown in Fig. 1(c), requires a numerical treatment of the electrostatics. We consider a case of strong forward bias in which a barrier layer limits hole transport at the metal/semiconductor interface and we treat the accumulation region in the semiconductor as a quasi-equilibrium system characterized by a Fermi energy for holes

with a valence band density of states N_V . The electrostatics in the accumulation region is determined by the hole density which is given by statistics:

$$p(x) = N_V \frac{2}{\sqrt{\pi}} \mathcal{F}_{\frac{1}{2}} [\lambda_F(x)] \quad (\text{A3})$$

where the Fermi one-half integral is given by

$$\mathcal{F}_{\frac{1}{2}} [y] = \int_0^\infty \frac{\lambda^{\frac{1}{2}}}{1 + e^{\lambda - y}} d\lambda \quad (\text{A4})$$

and

$$\lambda(x) = \frac{\varepsilon - E_V(x)}{kT} \quad \lambda_F(x) = \frac{E_F - E_V(x)}{kT}. \quad (\text{A5})$$

Far from the interface the hole density is equal to the acceptor doping level $p(\infty) = N_A$ so the local hole concentration can be written as

$$p(x) = N_A \frac{\mathcal{F}_{\frac{1}{2}} [\lambda_F(x)]}{\mathcal{F}_{\frac{1}{2}} [\lambda_F(\infty)]}. \quad (\text{A6})$$

To solve Poisson's equation, we compute the charge density by subtracting the background density of ionized accepters which yields

$$\begin{aligned} \rho(x) &= e[p(x) - N_A] \\ &= eN_A \frac{\mathcal{F}_{\frac{1}{2}} [\lambda_F(x)] - \mathcal{F}_{\frac{1}{2}} [\lambda_F(\infty)]}{\mathcal{F}_{\frac{1}{2}} [\lambda_F(\infty)]}. \end{aligned} \quad (\text{A7})$$

These algebraic steps are made so that the numerator can be rearranged to give an integral with a closed-form solution. First we rearrange the difference of Fermi integrals in the numerator as:

$$\begin{aligned} \mathcal{F}_{\frac{1}{2}} [\lambda_F(x)] - \mathcal{F}_{\frac{1}{2}} [\lambda_F(\infty)] \\ = \int_0^\infty \frac{\lambda^{1/2}}{1 + e^{\lambda - \lambda_F(\infty)}} \mathcal{A} d\lambda \end{aligned} \quad (\text{A8})$$

where

$$\begin{aligned} \mathcal{A} &= \frac{1 - e^{\lambda_F(\infty) - \lambda_F(x)}}{e^{\lambda_F(\infty) - \lambda} + e^{\lambda_F(\infty) - \lambda_F(x)}} \\ &= \frac{1 - e^{\frac{E_V(x) - E_V(\infty)}{kT}}}{e^{\lambda_F(\infty) - \lambda} + e^{\frac{E_V(x) - E_V(\infty)}{kT}}}. \end{aligned} \quad (\text{A9})$$

We substitute the charge density into the integral form of Poisson's equation for the electric field F . This process begins with Poisson's equation in the form

$$\int_{F(x)}^{F(\infty)=0} F dF = \int_{E_V(x)}^{E_V(\infty)} \frac{\rho(E_V)}{\varepsilon_s \varepsilon_o} dE_V \quad (\text{A10})$$

and results in

$$\begin{aligned} F^2(x) &= \frac{2N_A}{\varepsilon_s \varepsilon_o \mathcal{F}_{\frac{1}{2}} [\lambda_F(\infty)]} \\ &\times \int_0^\infty \frac{\lambda^{1/2}}{1 + \exp(\lambda - \lambda_\infty)} \left(\int_{E_V(x)}^{E_V(\infty)} \mathcal{A} dE_V \right) d\lambda \end{aligned} \quad (\text{A11})$$

which can be simplified by substituting the analytic expression for the interior integral. After substitution and simplification, we arrive at the following result:

$$\begin{aligned} F^2(x) &= \frac{2kTN_A}{\varepsilon_s \varepsilon_o \mathcal{F}_{\frac{1}{2}} [\lambda_F(\infty)]} \\ &\times \int_0^\infty \frac{\lambda^{1/2}}{1 + q} \left(\bar{q}q + (1 + q) \ln \left[\frac{1 + qe^{-\bar{q}}}{1 + q} \right] \right) d\lambda \end{aligned} \quad (\text{A12})$$

where \bar{q} and q are defined by

$$\bar{q} = \frac{E_V(\infty) - E_V(x)}{kT} \quad q = \exp(\lambda - \lambda_\infty). \quad (\text{A13})$$

An electrostatic profile is computed by first obtaining the electric field at $x=0$. Given the energy barrier (fixes \bar{q} at $x=0$) and doping density (fixes the fermi level relative to the band edge in the bulk), we can obtain $F(0)$ with one numerical integration of Eq. (A12). The valence band, electric field, and density profiles are then generated by integrating Eqs. (A10) and (A12) forward in x and evaluating Eq. (A7) at each spatial step. A sample result of this process is plotted in Fig. 8.

APPENDIX B: SOLUTIONS TO THE TRANSPORT EQUATION IN THE DEPLETION REGION

In this appendix we present analytic solutions for the transport equation (21) when the depletion approximation is used for the electrostatics of the structure.

In the depletion mode cases, we have a second order differential equation in the depletion region that is solved subject to boundary conditions at the metal/semiconductor interface and at the depletion region edge in the semiconductor. A typical equation, including the possibility of optical generation, can be written as

$$\frac{d^2\Omega}{dx^2} + \frac{e}{kT} \frac{d\phi}{dx} \frac{d\Omega}{dx} - \frac{1}{\Lambda^2} \Omega = -Ge^{-\frac{e\phi}{kT}}. \quad (\text{B1})$$

Within the depletion approximation, we have a quadratic form of the electrostatic potential

$$\frac{e\phi}{kT} = \frac{1}{2}ax^2 + bx + \frac{e\phi_o}{kT} \quad (\text{B2})$$

The particular solution Ω_p is

$$\Omega_p = \frac{G}{a + \frac{1}{\Lambda^2}} e^{-\frac{e\phi}{kT}} \quad (\text{B3})$$

and the homogeneous differential equation can be written as

$$\frac{d^2\Omega}{dx^2} + (ax + b) \frac{d\Omega}{dx} - \frac{1}{\Lambda^2} \Omega = 0. \quad (\text{B4})$$

Solutions results from a change of variables that transform the homogeneous differential equation to the confluent hypergeometric equation,

$$z \frac{d^2f}{dz^2} + (\xi - z) \frac{df}{dz} - \zeta f = 0, \quad (\text{B5})$$

which has independent solutions $M(\zeta, \xi, z)$ and $U(\zeta, \xi, z)$, the confluent hypergeometric functions of the first and second kinds.²⁰ In order to avoid the use of complex coefficients (this may arise if a single form of the solution is used with both directions of the electric field), we give the variable substitutions and homogeneous solutions Ω_h for n-type ($a < 0, b > 0$) and p-type ($a > 0, b < 0$) cases separately.

The necessary transformations are obtained by substituting

$$\Omega_h = (ax + b) f(z) \quad z = \frac{-(ax + b)^2}{2a} \quad (\text{n-type}) \quad (\text{B6})$$

or

$$\Omega_h = (ax + b) e^{-z} f(z) \quad z = \frac{(ax + b)^2}{2a} \quad (\text{p-type}) \quad (\text{B7})$$

into Eq. (B4). The result of the transformation is Eq. (B5) with $\xi = \frac{3}{2}$ and

$$\zeta = \frac{1}{2} - \frac{1}{2a\Lambda^2} \quad (\text{n-type}) \quad (\text{B8})$$

or

$$\zeta = 1 + \frac{1}{2a\Lambda^2} \quad (\text{p-type}). \quad (\text{B9})$$

In both the n-type and p-type solutions,

$$f(z) = \gamma_1 M(\zeta, \xi, z) + \gamma_2 U(\zeta, \xi, z) \quad (\text{B10})$$

where γ_1 and γ_2 are coefficients determined by applying boundary conditions.

Boundary conditions applied at the depletion edge where $x=w=-b/a$ require the evaluation of the special functions as the argument vanishes, $z \rightarrow 0$. The $M(\zeta, \xi, z)$ function approaches unity as z vanishes. The $U(\zeta, \xi, z)$ function is more

complicated. The small argument behavior of interest is given by

$$\lim_{z \rightarrow 0} U(\zeta, \xi, z) \sim \frac{\pi}{\sin(\pi\xi)} \times \left\{ \frac{1}{\Gamma(1 + \zeta - \xi) \Gamma(\xi)} - \frac{1}{z^{\xi-1} \Gamma(2 - \xi) \Gamma(\zeta)} \right\}. \quad (\text{B11})$$

The apparent singularity is cancelled by the leading factors of $(ax+b)$ in Eqs. (B6) and (B7). It can be shown after some algebra that the functions and derivatives have well behaved values at the depletion edge given by

$$\Omega_h(w) = \gamma_2 \frac{\sqrt{-2\pi a}}{\Gamma\left(\frac{1}{2} - \frac{1}{2a\Lambda^2}\right)} \quad (\text{n-type}) \quad (\text{B12})$$

or

$$\Omega_h(w) = -\gamma_2 \frac{\sqrt{2\pi a}}{\Gamma\left(1 + \frac{1}{2a\Lambda^2}\right)} \quad (\text{p-type}) \quad (\text{B13})$$

and

$$\left. \frac{d\Omega_h}{dx} \right|_{x=w} = a\gamma_1 + \gamma_2 \left[\frac{-2a\sqrt{\pi}}{\Gamma\left(\frac{1}{-2a\Lambda^2}\right)} \right] \quad (\text{n-type}) \quad (\text{B14})$$

or

$$\left. \frac{d\Omega_h}{dx} \right|_{x=w} = a\gamma_1 - \gamma_2 \left[\frac{2a\sqrt{\pi}}{\Gamma\left(\frac{1}{2} + \frac{1}{2a\Lambda^2}\right)} \right] \quad (\text{p-type}). \quad (\text{B15})$$

The other matching solutions occur for the interface at $x=0^+$ and require only the evaluation of the special functions for typical arguments with no special considerations.

-
- ¹ P. C. van Son, H. Kempen, and P. Wyder, Phys. Rev. Lett. **58**, 2271 (1987).
- ² Z. G. Yu and M. E. Flatte, Phys. Rev. B, **66**, 235302 (2002).
- ³ E. I. Rashba, Eur. Phys. J. B, **29**, 513 (2002).
- ⁴ D. L. Smith and R. N. Silver, Phys. Rev. B **64**, 045323 (2001).
- ⁵ E. I. Rashba, Phys. Rev. B **62**, 16267 (2000).
- ⁶ G. Schmidt, D. Ferrand, L. W. Molenkamp, A. T. Filip, and B. J. van Wees, Phys. Rev. B **62**, 4790 (2000).
- ⁷ A. G. Aronov and G. E. Pikus, Fiz. Tekh. Poluprovodn. **10**, 1177 (1976) [Sov. Phys. Semicond. **10**, 698 (1976)].
- ⁸ J. D. Albrecht and D. L. Smith, Phys. Rev. B **66**, 113303 (2002).
- ⁹ H. J. Zhu, M. Ramsteiner, H. Kostial, M. Wassermeier, H.-P. Schönherr, and K. H. Ploog, Phys. Rev. Lett. **87**, 016601 (2001).
- ¹⁰ A. F. Isakovic, D. M. Carr, J. Strand, B. D. Schultz, C. J. Palmstrom, and P. A. Crowell, Phys. Rev. B **64**, 016304 (2001).
- ¹¹ A. T. Hanbicki, B. T. Jonker, G. Itskos, G. Kioseoglou, and A. Petrou, Appl. Phys. Lett. **80**, 1240 (2002).
- ¹² B. T. Jonker, Y. D. Park, B. R. Bennett, H.-D. Cheong, G. Kioseoglou, and A. Petrou, Phys. Rev. B **62**, 8180 (2000).
- ¹³ R. Fiederling, M. Keim, G. Reuscher, W. Ossau, G. Schmidt, A. Waag, and L. W. Molenkamp, Nature (London) **402**, 787 (1999).
- ¹⁴ V. F. Motsnyi, J. De Boeck, J. Das, W. Van Roy, G. Borghs, E. Goovaerts, and V. I. Safarov, Appl. Phys. Lett. **81**, 265 (2002).
- ¹⁵ A. T. Hanbicki, O. M. J. van t Erve, R. Magno, G. Kioseoglou, C. H. Li, B. T. Jonker, G. Itskos, R. Mallory, M. Yasar, and A. Petrou, cond-mat/0302221 (11 Feb 2003).
- ¹⁶ R. M. Stroud, A. T. Hanbicki, Y. D. Park, A. G. Petukhov, B. T. Jonker, G. Itskos, G. Kioseoglou, M. Furis, and A. Petrou, Phys. Rev. Lett. **89**, 166602 (2002).
- ¹⁷ S. M. Sze, *Physics of Semiconductor Devices, second edition* (John Wiley & Sons, New York, 1981), p. 294.
- ¹⁸ G. L. Bir, A. G. Aronov, and G. E. Pikus, Sov. Phys.-JETP **42**, 705 (1976) [Zh. Eksp. Teor. Fiz. **69**, 1382 (1975)].
- ¹⁹ V. P. Varshni, Phys. Stat. Sol. **19**, 459 (1967); **20**, 9 (1967).
- ²⁰ L. J. Slater, in *Handbook of Mathematical Functions*, edited by M. Abramowitz and I. A. Stegun, (Dover Publications, Inc., New York, 1965), p. 504.